Classification: PHYSICAL SCIENCES - Anthropology

Title: Rome's urban history inferred from Pb-contaminated waters trapped in its ancient harbor basins

Author names: Hugo Delile[1,2,3*], Duncan Keenan-Jones[4], Janne Blichert-Toft[3], Jean-Philippe Goiran[1], Florent Arnaud-Godet[3], Francis Albarède[3]

Author affiliations:
[1] Maison de l'Orient et de la Méditerranée, CNRS UMR 5133, 69365 Lyon Cedex 7, France
[2] Department of Archaeology, University of Southampton, Avenue Campus, Southampton SO17 1BF, United Kingdom
[3] Ecole Normale Supérieure de Lyon, Université Claude Bernard-Lyon I, CNRS UMR 5276, 69007 Lyon, France
[4] Classics, School of Humanities, University of Glasgow, Glasgow, Lanarkshire, G12 8QQ, United Kingdom

***Corresponding author:** Hugo Delile, hugo.delile@mom.fr

Keywords: paleo-pollution, lead pipes, Pb isotopes, harbor geoarcheology, Rome, Ostia, Tiber

Abstract

Heavy metals from urban run-off preserved in sedimentary deposits record long-term economic and industrial development via the expansion and contraction of a city's infrastructure. Lead concentrations and isotopic compositions measured in the sediments of the harbor of Ostia – Rome's first harbor – show that lead pipes used in the water supply networks of Rome and Ostia were the only source of radiogenic Pb, which, in geologically young Central Italy, is the hallmark of urban pollution. High-resolution geochemical, isotopic, and ^{14}C analyses of a sedimentary core from Ostia harbor have allowed us to date the commissioning of Rome's lead pipe water distribution system to around the 2nd c. BC, considerably later than Rome's first aqueduct built in the late 4th c. BC. Even more significantly, the isotopic record of Pb pollution proves to be an unparalleled proxy for

tracking the urban development of ancient Rome over more than a millennium, providing the first semi-quantitative record of the water system's initial expansion, its later neglect, probably during the civil wars of the 1st c. BC, and its peaking in extent during the relative stability of the early-high Imperial period. The present core record fills the gap in the system's history before the appearance of more detailed literary and inscriptional evidence from the late 1st c. BC onwards. It also preserves evidence of the changes in the dynamics of the Tiber River that accompanied the construction of Rome's artificial port, Portus, during the 1st and 2nd c. AD.

Significance Statement

Isotopic evidence demonstrating that Rome's lead water pipes were the primary source of lead pollution in the city's runoff reveals the sedimentary profile of lead pollution in the harbor at Ostia to be a sensitive record of the growth of Rome's water distribution system and hence of the city itself. The introduction of this lead pipe network can now be dated to around the 2nd c. BC testifying to a delay of about a century and a half between the introduction of Rome's aqueduct system and the installation of a piped grid. The diachronic evolution of anthropogenic lead contamination is able to capture the main stages of ancient Rome's urbanization until its peak during the early-high Empire.

\body

Introduction

Recent cases of lead contamination of drinking water in the Midwestern United States have highlighted the sensitive equilibrium between essential urban water supply, hydraulic infrastructures, and economic and public health (1). Lead pollution was already affecting the urban waters of great Roman cities two millennia ago (2-4) although to a lesser extent than suggested earlier (5). Harbor sediment cores provide one of the best continuous records of human impact on the local environment. By combining isotopic analysis of lead in harbor sediments with evidence derived from archeological materials (e.g. lead pipes) and carbonates – known as travertine or sinter taken from aqueduct channels – recent studies have shown that the proportion of foreign lead in sediments constitutes a proxy for the expansion and contraction of the water supply system and therefore of urban development over the lifetime of a city (2-4). Urban centers were particularly vulnerable to the interruption of their water supply network due to natural or human causes (6). Hiatuses in the imported Pb isotopic record of the Trajanic basin sediments at Portus (core TR14, Fig. 1A), the maritime port of Imperial Rome, and those from the channel connecting Portus with the Tiber (Canale Romano, core CN1, Fig. 1A) reflect the 6th c. AD Gothic Wars and 9th c. Arab sack of Rome (2). The chronological record at Portus, however, only started with Trajan (AD 98-117), leaving the earlier history of Rome's urbanization essentially undocumented except for sparse archeological evidence and passing mentions in politically biased historical accounts. The same is the case for the development of Rome's water distribution network before the reforms of Agrippa in the late 1st c. BC (6), from which point on the admittedly problematic texts of Vitruvius (7) and Frontinus (Rome's water commissioner c. AD 100) (8) provide more information. The first Roman aqueduct, the Aqua Appia (late 4th c. BC) (6, 9), appears well

78 before any evidence of widespread usage of lead water pipes (*fistulae*, in the late 1st c. BC)
79 (10), raising the question of how water was distributed.
80 In order to explore these questions, we conducted a high-resolution analysis, including
81 the measurement of major and trace element concentrations and Pb isotopic compositions, of
82 a 12 m long sediment core (PO2, Fig. 1B) from Ostia. Ostia, today a featureless coastal plain
83 near the Tiber river (Fig. 1B), was the first harbor to serve Rome (11). The time span
84 encompassed by core PO2 is constrained by 15 radiocarbon dates covering the 1st millennium
85 BC (Table S1) (12). Lead concentrations and isotopic compositions also were measured on
86 sediments from the PTXI-3 core drilled at Portus in the basin of Claudius (AD 41-54) (Fig.
87 1A), the entry port of the Trajan basin, although at a coarser resolution than the PO2 core.
88

89 # Results

90 ## Stratigraphy

91 The stratigraphy of the PO2 core (Fig. 2A) can be subdivided into three main sedimentary
92 units, pre-harbor (A), harbor (B), and post-harbor (C). (i) *Unit A* is represented by bedded and
93 shelly grey sands with *Posidonia* attesting to a depositional environment of deltaic
94 progradation up to the middle of the 4th c. BC (12). (ii) *Unit B is further subdivided into two*
95 *subunits, B1 and B2. Subunit B1* forms the lower harbor sequence characterized by compact
96 dark grey silt suggestive of a quiet environment and lasting until the beginning of the 2nd c.
97 BC. (iii) *Subunit B2* forms the upper harbor sequence and contains levels of yellow sands
98 brought in by repetitive floods of the Tiber, which occurred from the 2nd c. BC to the 3rd c.
99 AD according to the ^{14}C age-depth model (Fig. 2A). (iv) *Unit C's* yellow bedded silts from
100 the 3rd c. AD onward represent floodplain deposits.

101 ## Lead concentrations and major and trace element systematics

Whole-rock Pb concentrations in the PO2 (Fig. 2A) and PTXI-3 cores (Fig. S1) vary by 1-2 orders of magnitude from their lowest values, and have means of 64 and 106 ppm, respectively. The lowest values are consistent with the natural Pb background level of 22 ppm of the Tiber delta sediments (13, 14). The Pb Enrichment Factor (EF_{Pb}), defined as the ratio of Pb to Al (a crustal major element) in the samples normalized to the same ratio in a crustal reference (e.g., Holocene Tiber delta sediments) (13, 14), monitors the excess of Pb relative to the natural environment (EF_{Pb} = 1 signifies no Pb excess). The evolution of this pollution index in the harbor deposits of Ostia (Fig. 2B) goes from (i) values slightly above the natural Pb background level at the base of the stratigraphic section in the pre-harbor unit A located between 12 and 9 m core depth, with a mean EF_{Pb} of ~ 2.2, to (ii) values highly above the natural Pb background in the harbor subunit B2 (between ~ 6 and 3 m core depth, mean EF_{Pb} ~ 3.8) with three major peaks reaching EF_{Pb} values between 7 and 9. The other units of the core (subunit B1 and unit C) have EF_{Pb} values lower than 2.

The stratigraphic record of Pb concentrations varies in concert with the presence of detrital material, magnetic susceptibility and, to a lesser extent, the median grain size (Fig. 2B). The EF_{Pb} peaks in subunit B2 attest to a high-energy regime of fluvial activity (gray shadings in Fig. 2B). Factor Analysis of major and trace element abundances clearly identifies the siliciclastic component with terrigenous elements such as the rare-earth elements, K, Mn, and Ba as the first factor (F1, Figs. 2B, S2 and Table S2). Lead concentrations of the *bulk* sediment are tightly associated with F1 (Fig. 2B, r = -0.66 between EF_{Pb} and F1), which emphasizes that the terrigenous fraction is the main carrier of this element. Factor 4 (F4) inferred from the Factor Analysis opposes Na to heavy metals such as Pb, Sn, and Cd (Figs.2B, S2 and Table S2). The strong influence of Na within the stratigraphy reflects either the salinity of the harbor itself or the invasion of the sediments by the salt wedge, at the expense of anthropogenic material carried by the Tiber. For the Trajanic harbor as well as for

Ostia harbor, the association of the ostracodal marine group with high sediment Na contents is clear evidence of a marine-dominated environment (11, 14, 15).

Lead isotope compositions

The labile Pb can be broken down into three well-defined components. In Fig. 3, the $^{204}Pb/^{206}Pb$ vs $^{208}Pb/^{206}Pb$ vs $^{207}Pb/^{206}Pb$ 3D plot shows an apparently ternary mixture between geologically 'recent' Pb (components α' and α") and 'old' Pb (component β). The recent natural Pb is a mixture of volcanic Pb from the Alban Hills (component α') and sedimentary Pb from the Mediterranean outflow water (component α" present in local carbonate sediments) well separated by different $^{208}Pb/^{206}Pb$ values (2). The exact isotope compositions of the natural components α' and α" (Table S3) are somewhat arbitrary, but their specific assignment does not affect the conclusions reached about the order of magnitude and relative variations of the anthropogenic component β (see Table S4 for the Pb isotope composition of β).

The anthropogenic origin of the 'old' Pb that dominates subunit B2 (Figs. 4 and 5) can be demonstrated by converting the Pb isotope compositions into their corresponding geochemically informed parameters, which are the Pb model age T_{mod} and the $^{238}U/^{204}Pb$ (μ) and $^{232}Th/^{238}U$ (κ) ratios (Table S4) using the equations given by Albarède et al. (16). The advantages of this representation over that based on raw Pb isotope ratios have been demonstrated in a number of geological and (geo)archeological contexts (2-4, 16-19). In the present case, Peninsular Italy is a geologically young mountain range (T_{mod} < 30 Ma); the presence of Hercynian Pb (T_{mod} > 200 Ma) in Ostia sediments therefore unambiguously signals contamination of local waters by foreign Pb, likely lead artifacts (Figs. 3 and 4). Quantitative breakdown of Pb isotopes into natural and anthropogenic components as proposed by Delile et al. (2) essentially reproduces the contamination patterns visible in the T_{mod} record of Ostia.

To characterize the evolution of the anthropogenic Pb signal, we use another pollution index "f_β", which is based on the proportion of the anthropogenic β component in the Ostia sediments (see Methods section for equation details). Beyond some minor trends, the EF_{Pb}, $^{206}Pb/^{207}Pb$, T_{mod}, and f_β records (Fig. 5) largely correlate, showing that the anthropogenic component does not fluctuate randomly but displays robust peaks and troughs.

Discussion

Natural and anthropogenic Pb sources

In Figs. 3 and 4, the pre-harbor and early harbor samples from Ostia (core PO2) and Portus (cores TR14, CN1, and PTXI-3) plot along the mixing line between the two local sub-components α' and α". The sandy pre-harbor sediments (unit A of core PO2 and most of core PTXI-3) show consistently higher values of $^{208}Pb/^{206}Pb$ (Fig. 4A) and κ (Fig. 4B) than the harbor sediments highly dominated by clays and silts (harbor subunit B1). This can be explained by changes in mineral sorting processes resulting from varying hydrodynamic levels. According to Garçon et al. (20), some heavy minerals concentrated in coarse sediments are extremely radiogenic, allowing sandy sediments to reach higher $^{208}Pb/^{206}Pb$ values (20) and thus higher values of κ (r of $^{208}Pb/^{206}Pb$ vs $\kappa \sim 0.7$).

The intersection of two additional mixing lines – between α' and α" and the third anthropogenic component β – reveals that β is Hercynian in age ($T_{mod} \sim 325$ Ma) and characterized by high $^{204}Pb/^{206}Pb$ (~ 0.0546) (Fig. 4). [H1]Sediments located on the mixing line α'-β correspond to Pb-contaminated particles that were transported in turbulent conditions, explaining their presence exclusively in the sandy subunit B2. In contrast, sediments falling along the α"-β trend were deposited under quieter hydrodynamic conditions, typically the silty floodplain deposits of unit C. Nevertheless, the whole of the Portus (cores TR14, CN1, and

PTXI-3) and Ostia (core PO2) sediments (n = 177) affected by lead pollution converges towards the same distinct source, or mix of sources, of imported lead.

In Roman times, a substantial number of ships' hulls were sheathed -with large mm-thick lead plates to protect their submerged portions against fouling and corrosion (21). Lead plates, anchors, and sounding-lead weights are, however, unlikely to have been significant contributors to the anthropogenic Pb signal of Ostia sediments. The reasons for this are several. First, in seawater, lead passivation by the deposition of a film of chlorides and carbonates is fast and efficient (22). Second, because the earliest wreck with a hull sheathed in lead discovered so far dates to the mid-4th c. BC (23) and the practice had reached a peak by the end of the 4th c. BC (21), if the sheathing of ship's hulls were a significant lead pollution source, we would expect an excess of lead to be recorded in the functional harbor unit B1, which covers the 4th and the 3rd c. BC. Such lead pollution does not occur, however, until the harbor unit B2, which was deposited at the end of the use of the harbor (11, 15), from around the 2nd c. BC. In the same way, the practice of lead sheathing of ship's hulls was no longer significant from the middle of the 1st c. AD (21), while Pb pollution of Rome's harbor water column lasts until the 9th c. AD (2). Third, and most importantly, the anthropogenic component β is clearly homogenous (Figs. 3 and 4) (2). This is inconsistent with local contamination by a fleet covered in lead plates of a variety of origins, but consistent with distant sources well-mixed during the journey from Rome down the Tiber. Remarkably, the isotope abundances of component β match those of *fistulae* from the Roman urban water supply system (Figs. 3 and 4). The persistence of contamination for well over a millennium (200 BC to AD 800) and the uniqueness of its isotopic composition argue against random pollution. They rather suggest that a mechanism existed upstream from Ostia that efficiently mixed the isotopic compositions of all sources of anthropogenic Pb contributing to the anthropogenic signal so visible in the harbor sediments. Judging from the 20th c. mean flow

(230 m^3/s, 24), around 3% (7 m^3/s) of the Tiber's water was running through Rome's aqueducts at the peak of the Roman Empire (8, 25), a significant fraction of which passed through *fistulae*. Lead from Rome *fistulae* therefore seems the only acceptable source of contamination in Ostia sediments.

Our previous research into the source(s) of the imported Pb component of Rome *fistulae* highlighted the Roman mining districts in Western Europe (Spanish Sierra Morena, the English Pennines, the German Eifel, or the French Massif Central) (2). It is not clear whether the Pb ores derive from a single provenance or a mix of these regions, but recycling and salvaging practices of lead implemented by Romans (6, 10, 26) favor a mixture from several Hercynian sources. Such recycling would have contributed significantly to the stability of the isotopic signature of the imported Pb component over the long period observed. Additionally, the conspicuous isotopic stability in turn argues for long-term stability in the lead trade networks between Rome and the western half of its Empire.

Control factors of Pb content

Changes in two main processes control the variation in the Pb contents of the PO2 core: (1) the input of Pb in the hydrological system upstream of the core, and (2) the transport of that Pb to the PO2 site. The major change in Pb inputs is the construction of the piped water distribution system in Rome. The imported Pb of Rome's pipes (with older, Hercynian T_{mod} values) is progressively dissolved and transported down the Tiber to be deposited in the B2 and C units, except during disruptions to flow in the piped system occasioned by damage or neglect during political unrest, epidemics, natural disasters, etc. Regarding transport, there are two processes at work (flooding by contaminated river water and dilution by uncontaminated seawater) connected with Factors 1 and 4, respectively.

The correlation of EF_{Pb} with particle size, as well as with the magnetic susceptibility and F1, shows that Pb excesses in the bulk sediment trapped in the harbor basin of Ostia were

associated with Tiber flooding episodes that acted as a transport vector of Pb pollution. In other words, a period of increased river discharge (e.g. flooding) resulted in deposition of larger amounts of larger particles, and hence deposition of more Pb.

In subunit B2, T_{mod} (representing imported Pb in the labile rather than the bulk fraction) is not correlated with F1 (r = 0.09) but is correlated with F4 (r = 0.6). F4 is dominated by heavy metals such as Sn and Cd, which, like T_{mod}, signal anthropogenic influence, and which are opposed to Na (Fig. S2). Between 250 and 500 cm, several striking drops in Pb contamination levels occur (see $^{206}Pb/^{207}Pb$ in Fig. 5A), which consistently are accompanied by steep marine (F4) peaks (Fig. 2B). It therefore appears that sudden, uncontaminated seawater inputs into the harbor basin invariably resulted in a decrease in Pb pollution, probably due to a dilution effect. Dilution by an uncontaminated source of water is commonly observed in both ancient harbors, for example Sidon (27), and fluvial environments, such as the Ruhr river, a tributary to the Rhine (28), the Caima River (Portugal) (29), and the Belle Fourche River (USA) (30).

A chronology of lead pollution and Roman urbanism

It should first be emphasized that ^{14}C chronology is particularly imprecise for the time interval covering the Roman Republic and Empire. Supplemental figure S3 reports errors on calendar ages from 250 BC to AD 250 using the values of Reimer et al. (31). For a given value of ^{14}C age, the range and occasionally the multiplicity of possible calendar ages in this interval is large and uncertainties cannot be unambiguously represented by a single error interval. It also must be borne in mind that short-term fluctuations cannot be resolved in harbor sedimentary records, which average over several decades or more. Thus we here have cautiously linked the Pb isotope records only to longer-term historical events. Despite this caveat, four main periods nevertheless can be distinguished from Fig. 5.

- *Uncontaminated environment ($8^{th}/9^{th}$ - 2^{nd} c. BC).* From the bottom of the core to -563 cm (units A and B1) anthropogenic lead is not visible, even in harbor subunit B1, which dates from the foundation of Ostia in the 4th or early 3rd c. BC (32) to the beginning of the 2nd c. BC. Figure 5 shows that contamination is not detected until the 2nd c. BC. This underscores once more that Pb pollution derives primarily from the dissolution of *fistulae* (Figs. 3 and 4). Lead *fistulae* would not be expected at Ostia in this period, since Ostia relied on wells for its water supply until the first half of the 1st c. AD (33). The water of the Aqua Appia and Anio Vetus aqueducts at Rome, built, respectively, in the late 4th c. and early 3rd c. BC, were distributed by a lead-free system of masonry channels or terracotta or wooden pipes of which only few have been found. It seems likely that these aqueducts supplied only a small number of focal points in the city, perhaps centrally located public fountains. Such a minimalist system was a far cry from that of Imperial Rome, which supplied hundreds of baths and private residences through a complex network of *fistulae* (10).

- *Manifestation of anthropogenic Pb (basal part of subunit B2).* The next period (Fig. 5) is characterized by the first rise of anthropogenic Pb excesses in the sandy harbor subunit B2. The age-depth models of cores PO2 (Fig. 2A) and PTXI-3 (Fig. S1 and Table S1) both suggest that Pb contamination began around the 2nd c. BC.

This radiocarbon-based age-depth model receives some confirmation from scattered mentions in textual sources. The first dated stamps on lead pipes do not appear at Rome until 11 BC (10) and even later at Ostia (AD 37-41) (33-35). *Fistulae* seem to have been in use in water systems at the beginning of the 1st c. BC in Rome (36), however, and by the late 2nd century BC at nearby Alatri (10). Rome's system of public water basins and private connections was probably in operation by 184 BC, but lead pipes are not mentioned (9, 37). Already Cato the Elder (234-149 BC) (38) used the word *fistula* as meaning "pipe".

The high-resolution Pb isotopic characterization of core PO2 provides continuous and detailed insight into water supply and urbanization upstream. Following the first appearance of anthropogenic Pb in the harbor sediments of Ostia at -563 cm, the trend of decreasing $^{206}Pb/^{207}Pb$, $^{208}Pb/^{204}Pb$, $^{207}Pb/^{204}Pb$, $^{206}Pb/^{204}Pb$ (Fig. 5A), and μ (Fig. 5B) with time, as well as increasing EF_{Pb}, T_{mod}, and f_{β} (Fig. 5B) argues for an overall increase of the imported Pb component. Like at other Roman cities (4, 34), this trend reflects the increase in the geographic extent and/or density of the lead pipe system as a result of urban development. At Rome, it is consistent with the repair and expansion of the water supply system that accompanied the commissioning of the Aqua Marcia (late 140s BC) and Aqua Tepula (125 BC) aqueducts (6).

Then, a sudden drop in EF_{Pb}, T_{mod}, and f_{β}, and a sharp spike in $^{206}Pb/^{207}Pb$, $^{208}Pb/^{204}Pb$, $^{207}Pb/^{204}Pb$, $^{206}Pb/^{204}Pb$, and μ take place between -536 and -506 cm core depth (bottom gray band in Fig. 5A and B), corresponding to the 1st c. BC or early 1st c. AD. After the Aqua Tepula, a century of rampant unrest and outright civil war prevented aqueduct construction and hampered maintenance (6). The Ostia PO2 core thus provides the first evidence of the scale of the contemporaneous reduction in flows in Rome's lead pipe distribution system – of the order of 50% – resulting in decreased inputs of lead-contaminated water into the Tiber. Octavian (Augustus)'s progressive defeat of his rivals during the 30s BC (39) allowed his future son-in-law, Agrippa, to take control of Rome's water supply between 40 BC (40) and 33 BC (6). Over the next 30 years, they repaired and extended the existing aqueduct and *fistulae* system, as well as built an unprecedented three new aqueducts (6, 10), leading to renewed increase in Pb pollution of the Tiber river. This sequence of events is recorded as a sharp decrease in $^{206}Pb/^{207}Pb$, $^{208}Pb/^{204}Pb$, $^{207}Pb/^{204}Pb$, $^{206}Pb/^{204}Pb$ (Fig. 5A), and μ (Fig. 5B) accompanied by a major spike in EF_{Pb}, T_{mod}, and f_{β} (Fig. 5B) between -506 and -472 cm core.

While the correlation between politics, stability, and lead isotopic composition is clear, the precise mechanism behind this correlation is undoubtedly complex and requires further study.

- *Variability in pollution level (late 1st c. BC/early 1st c. AD to post AD 250).* The next chapter in the PO2 core stretches from -472 to -294 cm, covering the Roman Imperial period. The end of this phase falls outside the dated portion of the core. The overall trend shows continuing but declining Pb pollution from a peak around the beginning of this period. This continued Pb pollution is consistent with the Pb isotopic compositions of sediments deposited during the High Roman Empire in the Claudian (core PTXI-3, Fig. S1) and Trajanic basins (cores TR14) (2) at Portus as well as the canal leading to them (core CN1) (2) where T_{mod} values are ~ 125-200 Ma and κ values are ~ 3.96-3.98 (2), both indicative of imported lead. These sustained levels of anthropogenic Pb in multiple cores confirm the picture from textual and archeological data that the aqueduct and lead pipe distribution system was generally maintained until at least the mid-3rd c. AD (41, 42, 10). Reduced dissolution of Pb due to insulation of the pipes by coating of a limestone deposit known as travertine (8) is unlikely to be a factor in this decline. Travertine deposits centimeters thick have been observed in many ancient aqueducts, cisterns, fountains and pools, including those at Rome and Pompeii. The deposition process is driven by an excess of calcium carbonate (limestone) in the water resulting from the escape of carbon dioxide to the atmosphere (degassing) (43). In aqueducts, cisterns, fountains and pools, there is good interaction between the air and the water, facilitating such degassing. In a pressurized piped system like the ones that distributed water at Rome and Ostia, however, the water fills the entire pipe, inhibiting degassing and travertine deposition. Pipe damage – mentioned by two legal sources at Rome (6, 44) – probably led to regular replacement, thereby exposing fresh, uncoated lead for dissolution. The relative lack of travertine in pressurized pipes is borne out by our field observations at Rome (2) and

around the Bay of Naples (45, 46) where almost all parts of the system are coated in travertine except the pressurized pipes. Likewise, at Patara in Turkey (43), the pressurized inverted siphon pipes have much thinner travertine deposits than surrounding areas of the aqueduct. The travertine deposits from Pompeii (45) and the nymphaeum of Trajan at Ephesus (47) show elevated levels of lead that was clearly derived from the lead pipes and fittings, despite the widespread presence of travertine deposits in the systems. At Ostia, the situation is more complex: early lead contamination of travertine disappeared. The authors posit a change in water source (48)

The smooth declining trend in core PO2 is punctuated by two further dips in Pb pollution, the 2nd and 3rd in the core (middle and top gray bands in Fig. 5A and B). The 2nd decrease occurs from -470 to -440 cm (sometime between the late 1st c. BC and 1st c. AD) and the 3rd from -370 to -350 cm (sometime from the 1st c. to the early 3rd c. AD). Instability of the Tiber's flow regime is excluded as a cause for these drops because of the lack of correlation between f_β and F1 (r = 0.2 in subunit B2). These decreases coincide with two strong marine (F4) peaks (Fig. 2B)[H2], suggesting the most likely cause is the diversion of the contaminated Tiber water away from Ostia's harbor. Man-made links between the Tiber and the sea upstream of Ostia were constructed in this period: the northern canal, the Canale Romano, and the Claudian basin at Portus (mid-1st c. AD) followed by the Trajanic basin and probably the north-eastern canal (early 2nd c. AD) (49). These reductions in Tiber outflow would have initially and mechanically (i) brought less anthropogenic Pb and (ii) allowed more uncontaminated seawater to enter the harbor of Ostia, diluting the reduced Tiber-derived Pb. This would also explain why clear evidence of these anthropogenic Pb drops is not seen in the TR14 and CN1 cores (2). We cannot rule out, however, that the 2nd and 3rd drops in Pb pollution may be due to damage or neglect of the water distribution system.

After the second drop (-470 to -440 cm), the renewed rise in Pb excesses shows that the Pb concentration in the water recovered to a level only slightly below the previous peak, while the values of f_β recovered to levels consistent with imported lead being the source (Fig. 5B). Once the third drop passed (~ -350 cm), the lead pollution in the harbor water column returned to approximately two-thirds (f_β ~ 0.3-0.5) (Fig. 5B) of that of the major spike, with a surge of older Pb in leachates (~ 125-175 Ma) and a dramatic drop in the $^{206}Pb/^{207}Pb$, $^{208}Pb/^{204}Pb$, $^{207}Pb/^{204}Pb$, $^{206}Pb/^{204}Pb$ (Fig. 5A), and μ (Fig. 5B) derived from leaching of the *fistulae*. This last and durable Pb pollution phase recorded in the upper part of the PO2 core shows that maintenance of a somewhat reduced water system continued.

- *Decrease of the pollution level (post-AD 250).* The last period, post-dating AD 250, is characterized by a decrease in imported lead (f_β ~ 0.2 in the unit C, Fig. 5B). This decrease is also observed at the same time in the TR14 and CN1 cores at Portus (2) and is not associated with a strong period of marine influence (F4, Fig. 2B). It thus represents a contraction of the effective water distribution system at Rome, likely related to the increase in instability beginning in the 3rd c. AD. Indeed, after the mid 3rd c. AD,, no more aqueducts were built and maintenance was on a smaller scale (41), while no pipe stamps can be dated to the period from the mid-3rd to mid-4th c. AD (10). This period of receding Pb contamination corresponds to the apparent decline of Pb and Ag mining (50) and of overall economic activity in the Roman Empire (51).

Materials and Methods

Major and trace element concentrations were determined by complete digestion of the bulk sediment, whereas Pb isotope compositions were measured only on the most labile fraction in order to emphasize the anthropogenic contribution. A large selection of major and trace

element concentrations were measured for the 12 m long Ostia core PO2 every 14 cm (86 samples) (Table S5), while only Pb concentrations were analyzed for 12 samples from core PTXI-3. All samples from both cores were additionally measured for their Pb isotope compositions.

Major and trace elements. After sieving at 63 µm, aliquots of 100 mg sediment were weighed into screwtop Savillex beakers and dissolved in a clean laboratory in laminar flow hoods using a 3:1:0.5 mixture of concentrated double-distilled HF, HNO_3, and $HClO_4$. The samples were left to attack at 120-130 °C for 48 h, then evaporated to dryness. Perchlorates were converted to chlorides by drying down with 6 M distilled HCl. The samples were redissolved in 2 ml concentrated distilled HNO_3, from which ~10 percent aliquots were further diluted to 2% HNO_3 and internal standards (10 ppm Sc for ICP-AES and 2 ppb In for Q-ICP-MS) added. Major elements were analyzed by ICP-AES (ICAP 6000) and trace elements by Q-ICP-MS (Agilent 7500 CX) at the Ecole Normale Supérieure de Lyon. The upper limit of blank contribution is negligible for major elements and <2 % of the sample content for trace elements. The data are listed in Table S5.

Lead isotope compositions. The same method as described in Delile (13) and Delile et al. (2-4) was used. After sieving at 63 µm, representative aliquots of 500 mg of sediment were weighed out into screwtop Savillex beakers, then leached with hot Suprapur chloroform to separate the labile, or anthropogenic, component of the Pb. A second leaching step was done with hot dilute double-distilled HBr. The two leachates were combined and evaporated to dryness. Lead from the leachates was then separated on anion-exchange columns using distilled 1 M HBr to elute the sample matrix and distilled 6 M HCl to elute the Pb. The sample residues after leaching were not analyzed in this work because the isotopic composition of the natural Pb background had already been determined previously (2, 13). Lead isotope compositions were measured by multi-collector ICP-MS (Nu Plasma 500 HR) at

the Ecole Normale Supérieure de Lyon using Tl doping and sample-standard bracketing (52, 53) and the values for NIST 981 of Eisele et al. (54). The total procedural Pb blank was < 20 pg. The external reproducibility of the reported Pb isotope ratios as estimated from the repeated (every two samples) runs of NIST 981 are 100-200 ppm (or 0.01-0.02%) for ratios based on 204 ($^{206}Pb/^{204}Pb$, $^{207}Pb/^{204}Pb$, $^{208}Pb/^{204}Pb$) and 50 ppm (or 0.005%) for $^{207}Pb/^{206}Pb$, $^{208}Pb/^{206}Pb$, and $^{207}Pb/^{208}Pb$. The Pb isotope data are listed in Table S4.

The proportion $f\beta$ of the β component in the leachate is calculated by least-squares using three sets of equations, e.g.:

$$(^{204}Pb/^{206}Pb)\ \alpha'\ f\alpha' + (^{204}Pb/^{206}Pb)\ \alpha''\ f\alpha'' + (^{204}Pb/^{206}Pb)\ \beta\ f\beta = (^{204}Pb/^{206}Pb)_{leach}$$

with similar equations for the $^{207}Pb/^{206}Pb$ and $^{208}Pb/^{206}Pb$ ratios. In these equations, f is the proportion of ^{206}Pb assigned to each component. A closure equation ensuring that all the f s sum to 1 must be added.

Acknowledgments

We thank the Soprintendenza Speciale per i Beni Archeologici di Roma e Sede di Ostia for the permission to drill core PO2 in the ancient harbor basin of Ostia and Philippe Telouk for ensuring that the mass spectrometers always worked. We further acknowledge the ARTEMIS-SHS program and radiocarbon laboratory of Lyon for carrying out the radiocarbon dating. The Young Scientist Program of the Agence Nationale de la Recherche (CNRS) (ANR 2011 JSH3 002 01), the Roman Mediterranean Ports program (ERC grant agreement n° 339123), and the Ecole Française de Rome provided financial and logistic support. We are grateful to three anonymous reviewers and the editor whose insightful comments helped improve the manuscript.

References

1. Sherwin BD (2017) Pride and Prejudice and Administrative Zombies: How Economic Woes, Outdated Environmental Regulations, and State Exceptionalism Failed Flint, Michigan. University of Colorado law review 88(3).

2. Delile H, Blichert-Toft J, Goiran J-P, Keay S, Albarède F (2014a) Lead in ancient Rome's city waters. *PNAS* 111(18):6594–6599.

3. Delile H, et al. (2015) Demise of a harbor: A geochemical chronicle from Ephesus. *Journal of Archaeological Science* 53:202–213.

4. Delile H, et al. (2016) A lead isotope perspective on urban development in ancient Naples. *PNAS* 113(22):6148–6153.

5. Nriagu JO (1983) *Lead and Lead Poisoning in Antiquity* (John Wiley & sons, New York).

6. Frontinus SI (2004) De aquaeductu urbis Romae ed Rodgers RH (Cambridge University Press, Cambridge).

7. Lewis M (1999) Vitruvius and Greek aqueducts. *Papers of the British School at Rome* 67:145–172.

8. Keenan-Jones D, Motta D, Garcia MH, Fouke BW (2015) Travertine-based estimates of the amount of water supplied by ancient Rome's Anio Novus aqueduct. *Journal of Archaeological Science: Reports* 3:1–10.

9. Titus Livius (1835) Histoire romaine de Tite Live (C.L.F. Panckoucke, Paris, France).

10. Bruun C (1991) The water supply of Ancient Rome: a study of Roman imperial administration (The Finnish society of sciences and letters, Helsinki, Finlande).

11. Goiran J-P, et al. (2014) Geoarchaeology confirms location of the ancient harbour basin of Ostia (Italy). *Journal of Archaeological Science* 41:389–398.

12. Goiran J-P, et al. (2017) High chrono-stratigraphal resolution of the harbour sequence of Ostia: palaeo-depth of the bassin, ship drought & dredging. Journal of Archaeology: Supplementary Series (T. Franconi, Portsmouth), pp 67–83.

13. Delile H (2014) Signatures des paléo-pollutions et des paléoenvironnements dans les archives sédimentaires des ports antiques de Rome et d'Éphèse. Doctorat de géographie / géoarchéologie (Université Lumière Lyon 2, Lyon).

14. Delile H, et al. (2014b) Geochemical investigation of a sediment core from the Trajan basin at Portus, the harbor of ancient Rome. *Quaternary Science Reviews* 87:34–45.

15. Sadori L, et al. (2016) Palynology and ostracodology at the Roman port of ancient Ostia (Rome, Italy). *The Holocene*:1–11.

16. Albarède F, Desaulty A-M, Blichert-Toft J (2012) A geological perspective on the use of Pb isotopes in Archaeometry. *Archaeometry* 54(5):853–867.

17. Desaulty A-M, Telouk P, Albalat E, Albarède F (2011) Isotopic Ag–Cu–Pb record of silver circulation through 16th–18th century Spain. *PNAS* 108(22):9002–9007.

18. Bouchet RA, Blichert-Toft J, Reid MR, Levander A, Albarède F (2014b) Similarities between the Th/U map of the western US crystalline basement and the seismic properties of the underlying lithosphere. *Earth and Planetary Science Letters* 391:243–254.

19. Blichert-Toft J, et al. (2016) Large-scale tectonic cycles in Europe revealed by distinct Pb isotope provinces. *Geochemistry Geophysics Geosystems* 17(10):3854–3864.

20. Garçon M, Chauvel C, France-Lanord C, Limonta M, Garzanti E (2014) Which minerals control the Nd–Hf–Sr–Pb isotopic compositions of river sediments? *Chemical Geology* 364:42–55.

21. Kahanov Y (1999) Some aspects of lead sheathing in ancient ship construction. Tropis V, Hellenic Institute for the Preservation of Nautical Tradition. (Tzalas, H., Nauplia), pp 219–224.

22. Beccaria AM, Mor ED, Bruno G, Poggi G (1982) Corrosion of Lead in Sea Water. *British Corrosion Journal* 17(2):87–91.

23. Parker AJ (1992) Ancient shipwrecks of the Mediterranean & the Roman provinces (Tempus Reparatum, Oxford).

24. Millero, FJ, Macchi, G Pettine, M (1981). The speciation of ions in Tiber river estuary waters. *Estuarine, Coastal and Shelf Science* 13:517–534.

.

25. Blackman DR (1978) The Volume of Water Delivered by the Four Great Aqueducts of Rome. *Papers of the British School at Rome* 46:52–72.

26. Boni M, Maio GD, Frei R, Villa IM (2000) Lead Isotopic Evidence for a Mixed Provenance for Roman Water Pipes from Pompeii. *Archaeometry* 42(1):201–208.

27. Le Roux G, Veron A, Morhange C (2003) Geochemical evidences of early anthropogenic activity in harbour sediments from Sidon. *Archaeology & history in Lebanon* 18:115–119.

28. Moore JW, Ramamoorthy S, Ballantyne EE (1984) Heavy metals in natural waters: applied monitoring and impact assessment (Springer-Verlag, New York, Etats-Unis d'Amérique).

29. Ferreira da Silva E, et al. (2009) Heavy metal pollution downstream the abandoned Coval da Mó mine (Portugal) and associated effects on epilithic diatom communities. *Science of The Total Environment* 407(21):5620–5636.

30. Marron DC (1989) The transport of mine tailings as suspended sediments in the Belle Fourche River, West-Central South Dakota, U.S.A. *Sediment and Environment* (184):19–26.

31. Reimer PJ, et al. (2013) IntCal13 and Marine13 radiocarbon age calibration curves 0–50,000 years cal BP. *Radiocarbon* 55(4): 1869–1887.

32. Brandt JR (2002) Ostia and Ficana: Two Tales of One City? *Mediterranean Archaeology* 15:23–39.

33. Bukowiecki E, Monteix N, Rousse C (2008) Ostia Antica: Entrepôts d'Ostie et de Portus. Les Grandi Horrea d'Ostie. *Mélanges de l'Ecole française de Rome - Antiquité* 120(1):211–216.

34. Bruun C (2002) L'amministrazione imperiale di Ostia e Portus. Ostia e Portus nelle loro relazioni con Roma, Acta instituti romani finlandiae., eds Bruun C, Gallina A, Institutum Romanum Finlandiae (Institutum Romanum Finlandiae, Roma, Italie), pp 161–192.

35. Ricciardi MA, Scrinari VSM (1996) La civiltà dell'acqua in Ostia antiqua (Fratelli Palombi, Roma, Italie).

36. Cicero (1856) The orations of Marcus Tullius Cicero (H.G. Bohn, London).

37. Plutarch (1914) The Parallel Lives. Loeb Classical Library.

38. Cato MP (1934) On agriculture (W. Heinemann, London). Harvard University Press, Cambridge, Mass.

39. *Turchin* P, Scheidel W (2009) Coin hoards speak of population declines in Ancient Rome. PNAS 106(41):17276–17279.

40. Evans HB (1982) Agrippa's Water Plan. *American Journal of Archaeology* 86(3):401–411.

41. Van Deman EB (1934) The building of the Roman aqueducts (Carnegie institution of Washington, Washington, Etats-Unis d'Amérique).

42. Ashby T (1935) The aqueducts of ancient Rome ed Richmond I (Oxford University Press, Oxford).

43. Sürmelihindi G, Passchier CW, Baykan ON, Spötl C, Kessener P (2013) Environmental and depositional controls on laminated freshwater carbonates: An example from the Roman aqueduct of Patara, Turkey. *Palaeogeography, Palaeoclimatology, Palaeoecology* 386:321–335.

44. Pharr C, Davidson TS, Pharr MB (1952) *The Theodosian Code and novels and the Sirmondian constitutions* (Princeton University Press, Princeton).

45. Keenan-Jones D, Hellstrom J, Drysdale R (2011) Lead contamination in the drinking Water of Pompeii. Pompeii: Art, Industry and Infrastructure (E. Poehler, M. Flohr and K. Cole), pp 131–148. Oxbow books.

46. Keenan-Jones D (2010) The Aqua Augusta Regional water supply in Roman and late antique Campania. Dissertation (Macquarie University).

47. Prochaska W, Quatember U (2006) The Analysis of Sinter Samples and Hydraulic Mortars from the Nymphaeum Traiani at Ephesus. *Cura Aquarum in Ephesus* (Wiplinger, G., Ephesus/Selçuk, Turkey), pp 509–514.

48. Carlut J, Chazot G, Dessales H, Letellier É (2009) Trace element variations in an archeological carbonate deposit from the antique city of Ostia: Environmental and archeological implications. *Comptes Rendus Geoscience* 341(1):10–20.

49. Salomon F, et al. (2014) A harbour–canal at Portus: a geoarchaeological approach to the Canale Romano: Tiber delta, Italy. Water Hist 6(1):31–49.

50. Kylander M, et al. (2005) Refining the pre-industrial atmospheric Pb isotope evolution curve in Europe using an 8000 year old peat core from NW Spain. Earth and Planetary Science Letters 240:467– 485.

51. Scheidel W (2009) In search of Roman economic growth. Journal of Roman Archaeology (22):71–82.

52. White WM, Albarède F, Télouk P (2000) High-precision analysis of Pb isotope ratios by multi-collector ICP-MS. Chemical Geology 167(3–4):257–270.

53. Albarède F, et al. (2004) Precise and accurate isotopic measurements using multiple-collector ICPMS. Geochimica et Cosmochimica Acta 68(12):2725–2744.

54. Eisele J, Abouchami W, Galer SJG, Hofmann AW (2003) The 320 kyr Pb isotope evolution of Mauna Kea lavas recorded in the HSDP-2 drill core. Geochemistry, Geophysics, Geosystems 4(5):1–32.

55. Blaauw M (2010) Methods and code for "classical" age-modelling of radiocarbon sequences. *Quaternary Geochronology* 5(5):512–518.

56. Stumpf R, Frank M, Schönfeld J, Haley BA (2010) Late Quaternary variability of Mediterranean Outflow Water from radiogenic Nd and Pb isotopes. Quaternary Science Reviews 29(19–20):2462–2472.

57. Conticelli S, D'Antonio M, Pinarelli L, Civetta L (2002) Source contamination and mantle heterogeneity in the genesis of Italian potassic and ultrapotassic volcanic rocks: Sr–Nd–Pb isotope data from Roman Province and Southern Tuscany. Mineralogy and Petrology 74(2–4):189–222.

58. D'Antonio M, Tilton GR, Civetta L (1996) Petrogenesis of Italian Alkaline Lavas Deduced from Pb-Sr-Nd Isotope Relationships. Earth Processes: Reading the Isotopic Code, Geophysical monograph., eds Basu A, Hart S (Basu, A., Hart, S., Washington, D.C.), pp 253–267. American Geophysical Union.

Author Contributions

H.D. and J.-P.G. designed the project; J.-P.G. carried out the field work; H.D., J.B.-T. and F.A.-G. produced the data; H.D., D.K.-J., J.B.-T., J.-P.G. and F.A. analyzed and interpreted the data; H.D., D.K.-J., J.B.-T., and F.A. wrote the paper.

Figures

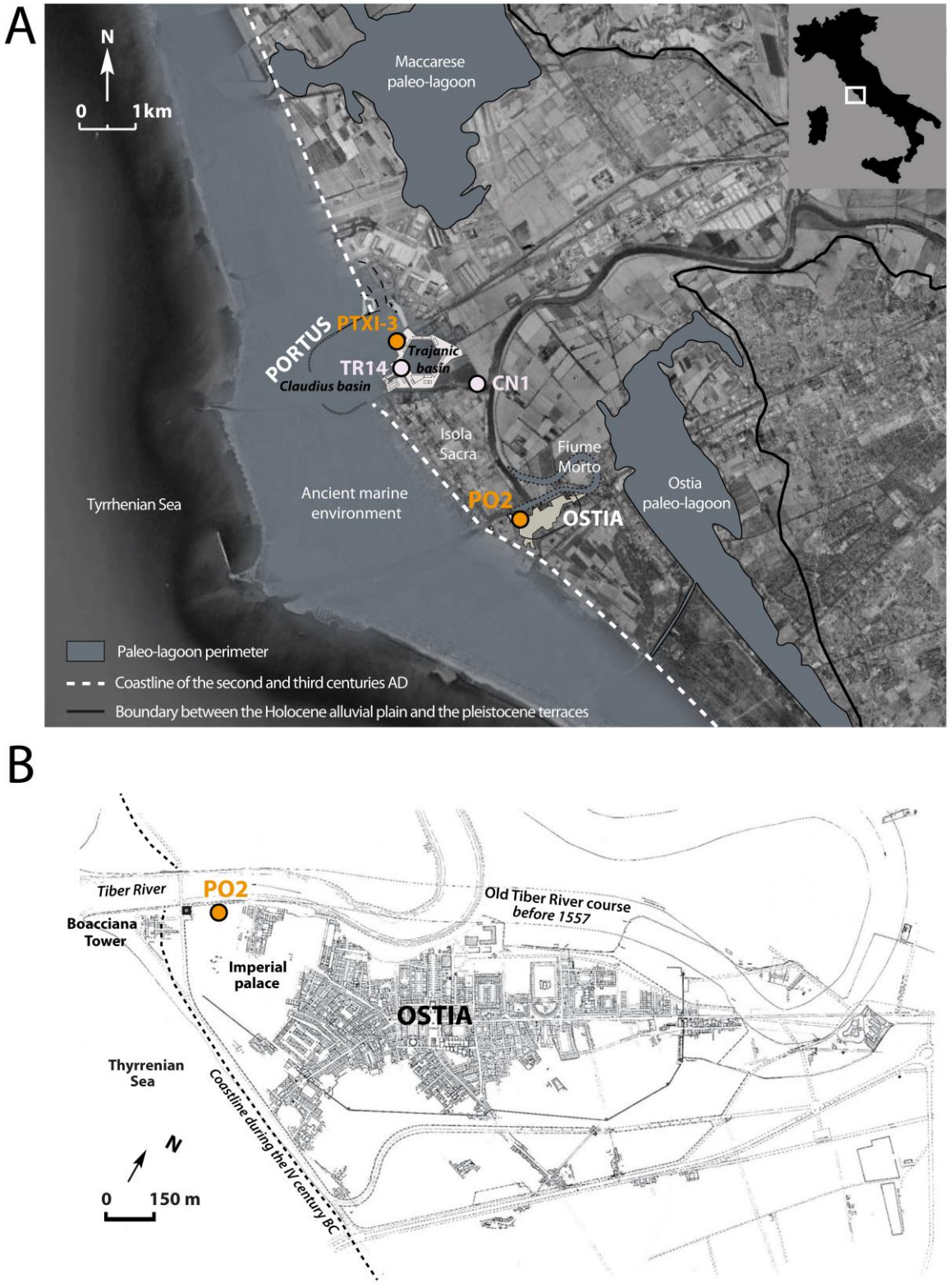

Fig. 1. (A) Location of ancient Rome's harbor basins in the Tiber delta with the position of cores PO2 and PTXI-3 (orange circles) analyzed in this work, and cores TR14 and CN1 analyzed by Delile et al. (2) (modified from ref. 11). (B) Map showing the archeological area

of ancient Ostia with the location of core PO2, as well as the old and the new Tiber river courses (modified from ref. 11).

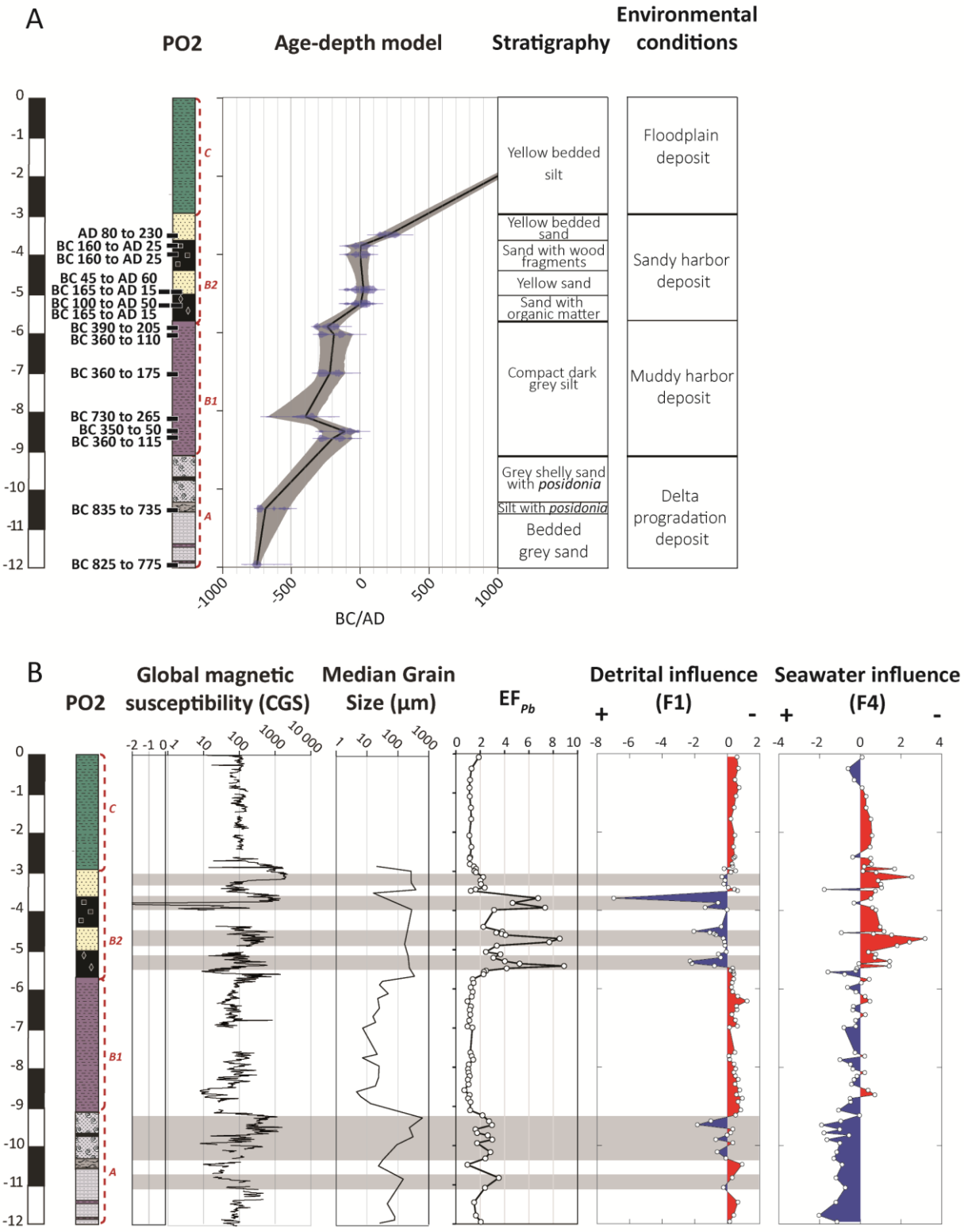

Fig. 2. Stratigraphic log of core PO2 showing (A) the age-depth model of the core constructed using the Clam software (55) from fifteen radiocarbon dates (symbolized by the black labels

on the stratigraphic log). Further details on the age-depth model and the ^{14}Cdates can be found in the captions to Fig. S3 and Table S1. The stratigraphic description of the core along with environmental interpretations are shown at the right-hand side; (B) the magnetic susceptibility values, the grain size 50 percentile (D 50) (11), the Pb enrichment factor (EF_{Pb}), and Factor 1 (detrital influence) and Factor 4 (seawater influence) of the Factor Analysis of major and trace element concentrations (see the detailed distribution of the individual elements in Fig. S2). The gray shadings highlight the synchronicity between the highest EF_{Pb} values, detrital activity in the harbor basin (negative values of F1), the grain size 50 percentile, and magnetic susceptibility.

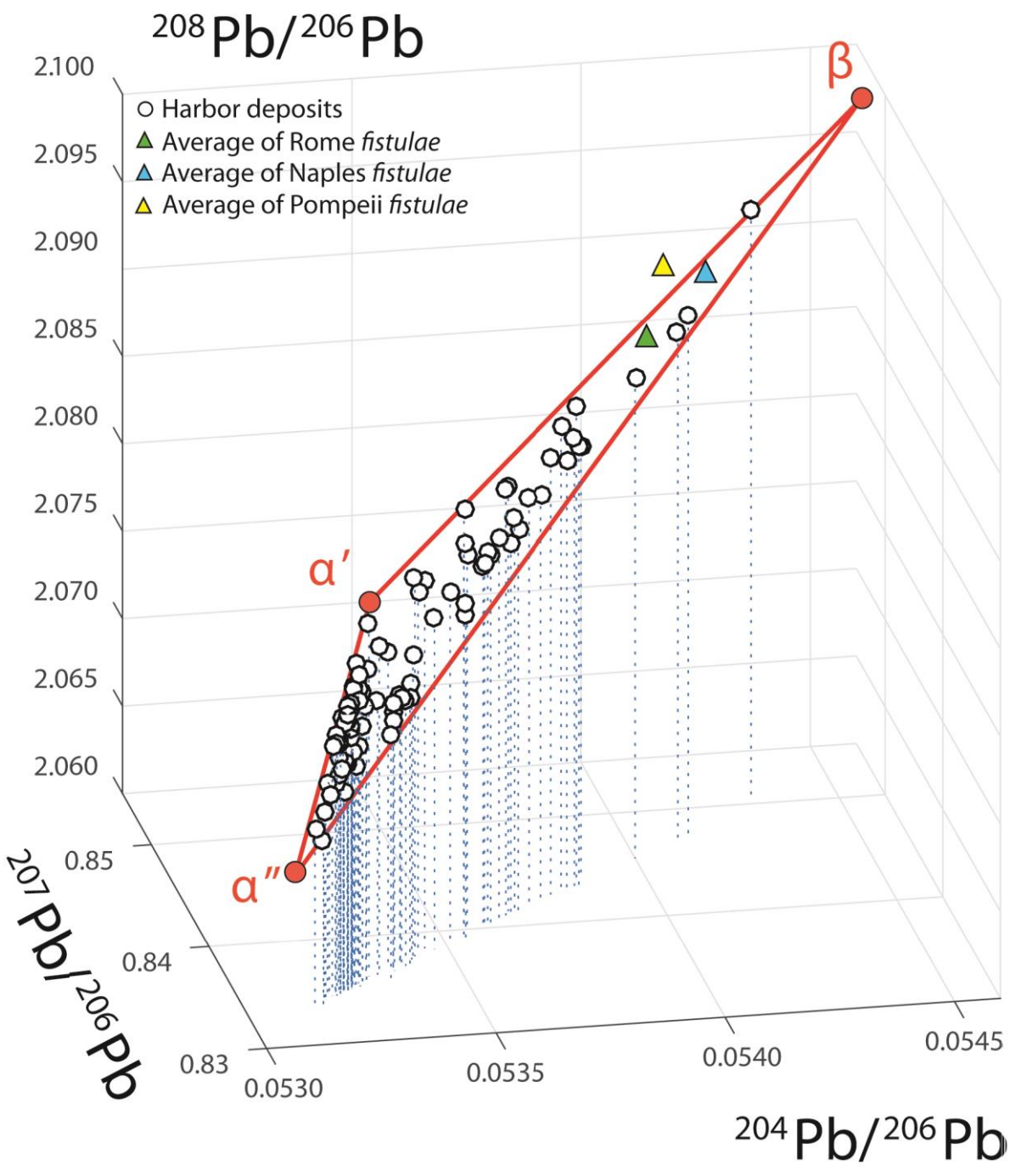

Fig. 3. 3D plot of $^{204}Pb/^{206}Pb$ vs $^{208}Pb/^{206}Pb$ vs $^{207}Pb/^{206}Pb$ measured on leachates from cores PO2 and PTXI-3. The track of the stippled blue drop lines suggests that the 3D data set as a whole could be interpreted as a single alignment in $^{207}Pb/^{206}Pb$ – $^{204}Pb/^{206}Pb$ space, and therefore as a two-component mixture.[h3] However, adding $^{208}Pb/^{206}Pb$ to the perspective demonstrates that lead is a mixture of three separate components, α', α", and β. The three red lines connect components α' and β, α" and β, and α' and α". The α' and α" mixing line

corresponds to unpolluted Tiber water and is composed of Mediterranean outflow water (α") (56) and volcanic rocks from the Alban Hills (α') (57, 58). β is the anthropogenic end-member located near the *fistulae* from Rome (2), Naples (4), and Pompeii (26).

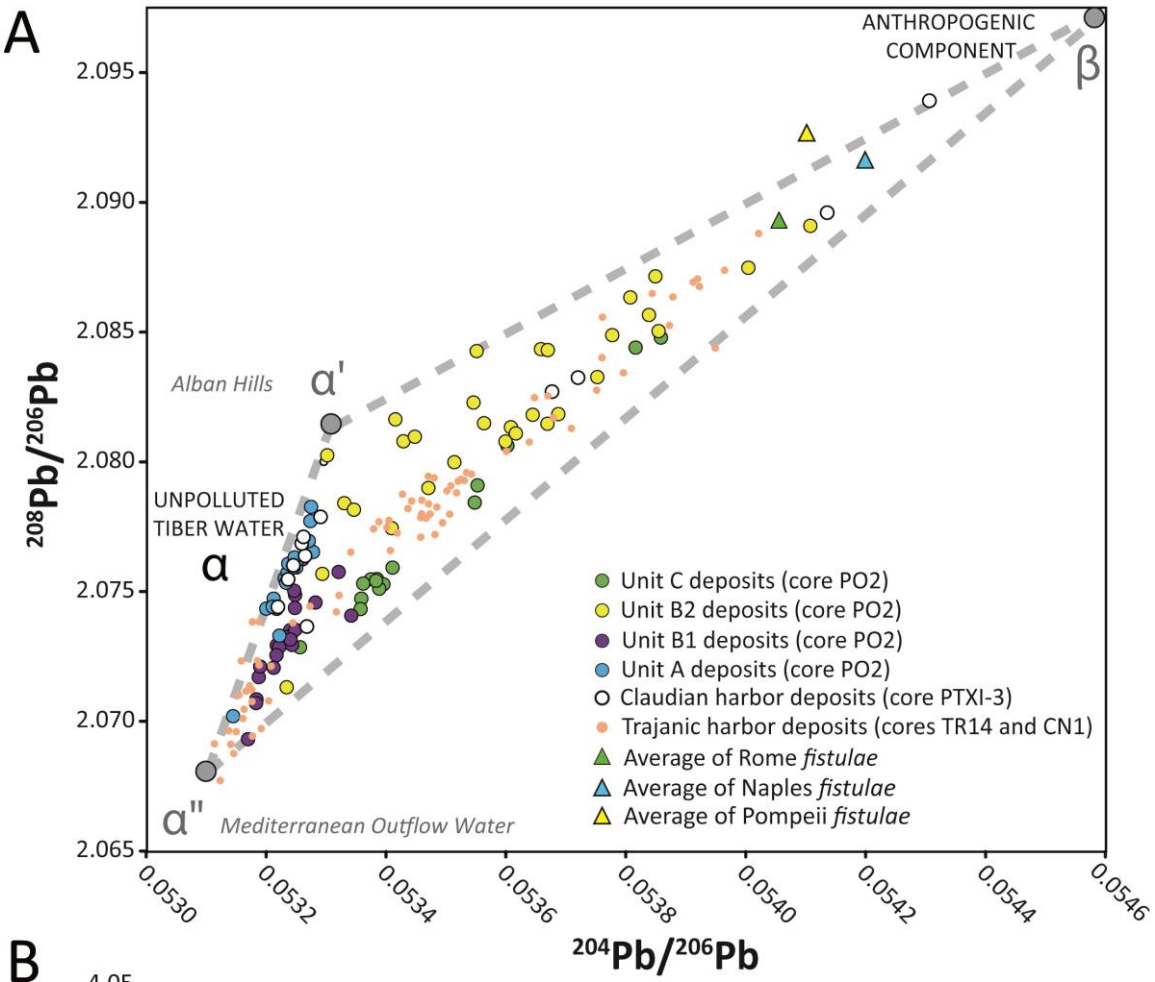
A
ANTHROPOGENIC
COMPONENT
β
Alban Hills
α'
UNPOLLUTED
TIBER WATER
α
α"
Mediterranean Outflow Water
Unit C deposits (core PO2)
Unit B2 deposits (core PO2)
Unit B1 deposits (core PO2)
Unit A deposits (core PO2)
Claudian harbor deposits (core PTXI-3)
Trajanic harbor deposits (cores TR14 and CN1)
Average of Rome fistulae
Average of Naples fistulae
Average of Pompeii fistulae
208Pb/206Pb
204Pb/206Pb
2.095
2.090
2.085
2.080
2.075
2.070
2.065
0.0530
0.0532
0.0534
0.0536
0.0538
0.0540
0.0542
0.0544
0.0546

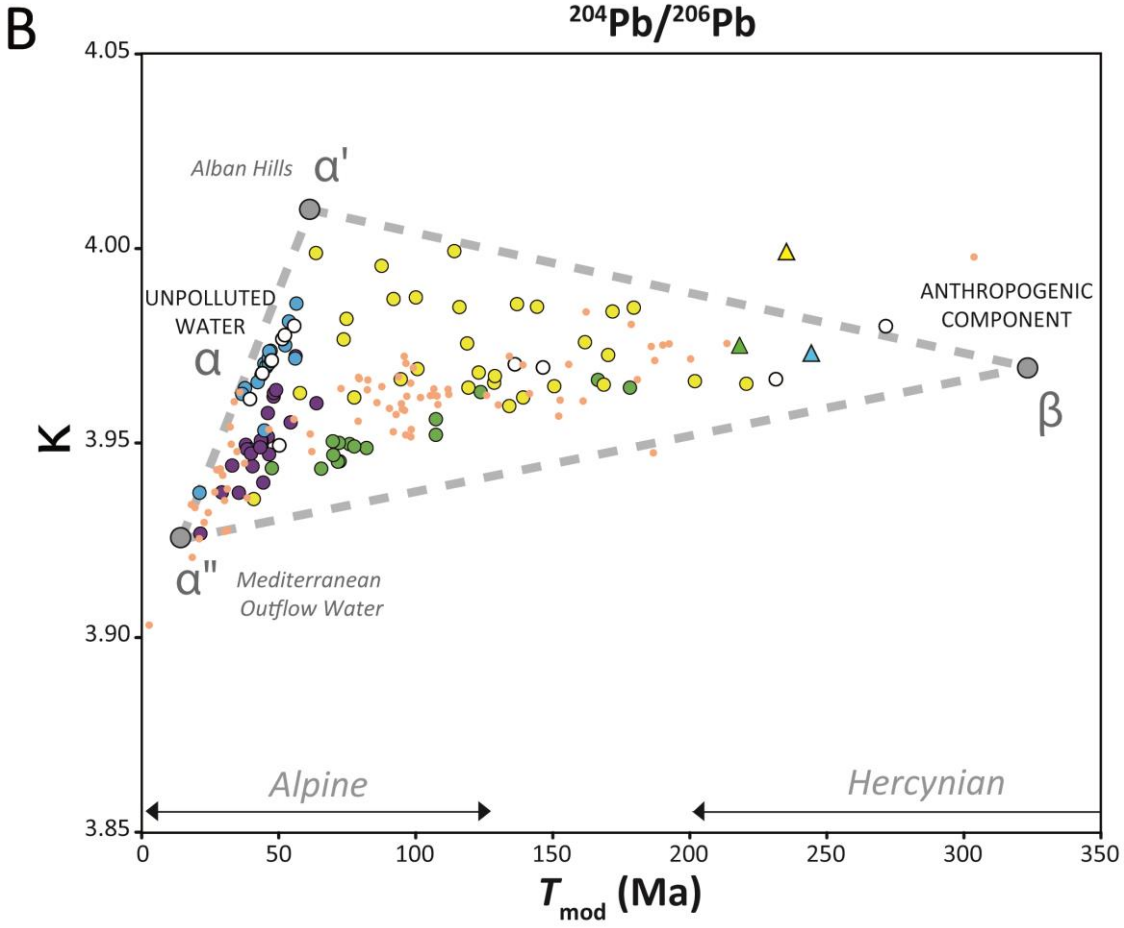
B
Alban Hills
α'
UNPOLLUTED
WATER
α
α"
Mediterranean
Outflow Water
ANTHROPOGENIC
COMPONENT
β
K
4.05
4.00
3.95
3.90
3.85
Alpine
Hercynian
0
50
100
150
200
250
300
350
T mod (Ma)

597

Fig. 4. Plots of (A) $^{204}Pb/^{206}Pb$ vs $^{208}Pb/^{206}Pb$ and (B) T_{mod} vs κ for leachates from cores PO2 (unit C in green, subunit B2 in yellow, subunit B1 in purple, unit A in blue), PTXI-3 (Claudian harbor), TR14 (Trajanic harbor), CN1 (Canale Romano deposits), and *fistulae* from Rome, Naples, and Pompeii (2, 4, 26).

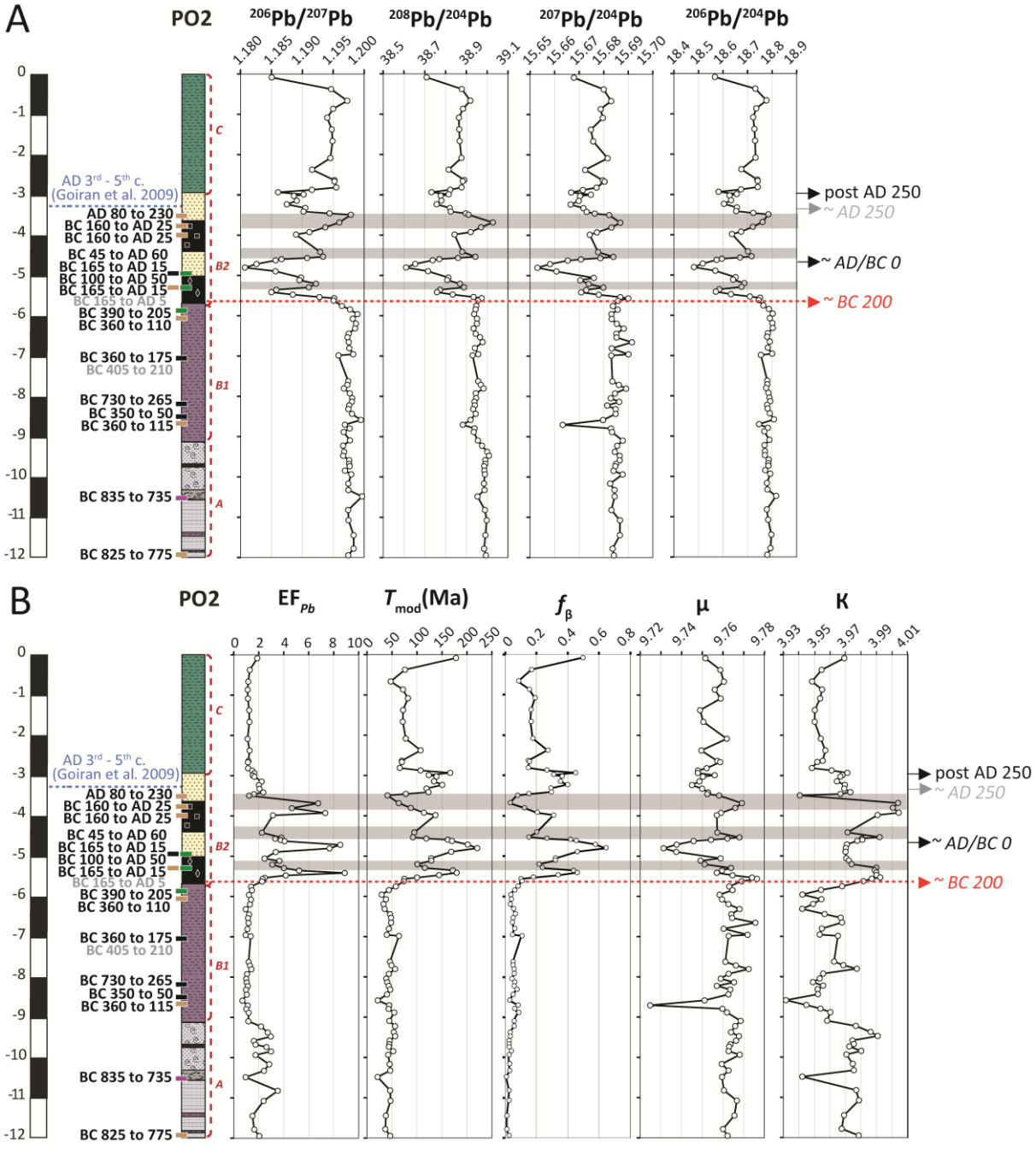

Fig. 5. Downcore variations of (A) $^{206}Pb/^{207}Pb$, $^{208}Pb/^{204}Pb$, $^{207}Pb/^{204}Pb$, and $^{206}Pb/^{204}Pb$ and (B) T_{mod}, f_{β}, μ, and κ. The red dotted line marks the first appearance of anthropogenic Pb pollution recorded in core PO2 from around 200 BC according to the age-depth model. The

gray bands show the main declining trends of anthropogenic lead pollution discussed in this study.

Supplementary Materials

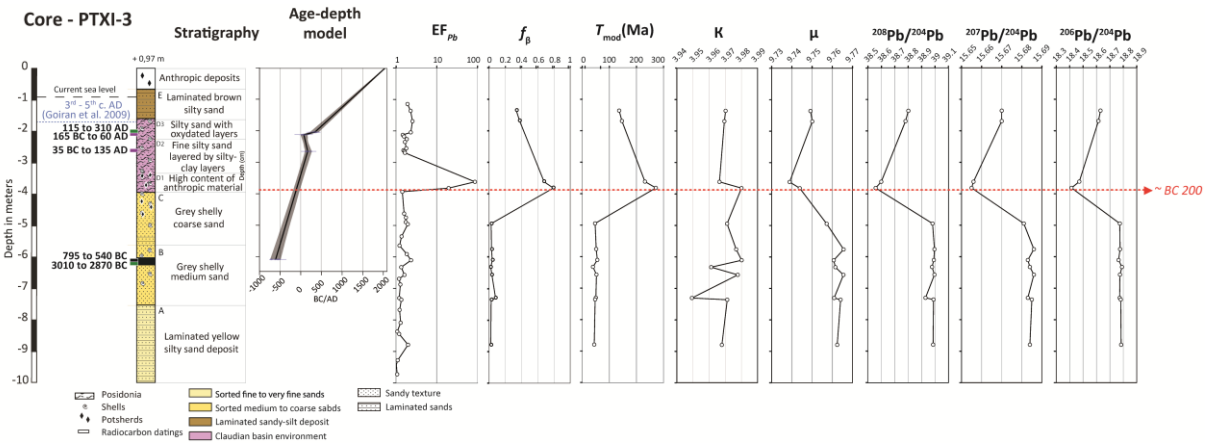

Fig. S1. Stratigraphic log of core PTXI-3 showing its stratigraphic description, ^{14}C dates, the age-depth model of the core constructed with the Clam software (55), EF$_{Pb}$, f_{β}, the geological parameters, and the Pb isotopic compositions.

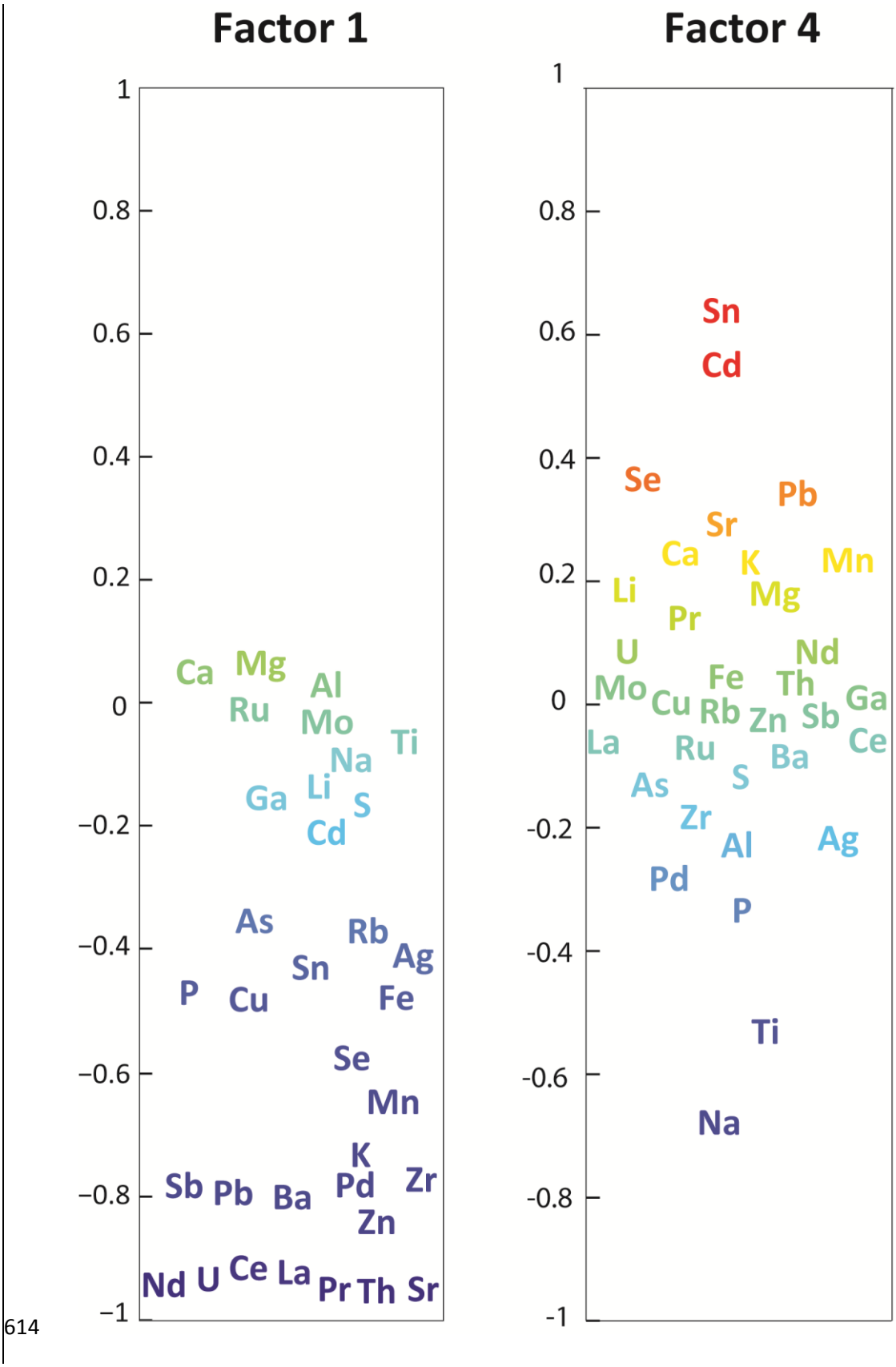
Factor 1
1
0.8
0.6
0.4
0.2
0
−0.2
−0.4
−0.6
−0.8
−1
Ca
Mg
Al
Ru
Mo
Ti
Na
Ga
Li
S
Cd
As
Rb
Ag
Sn
P
Cu
Fe
Se
Mn
K
Sb
Pb
Ba
Pd
Zr
Zn
Nd
U
Ce
La
Pr
Th
Sr
Factor 4
1
0.8
0.6
0.4
0.2
0
-0.2
-0.4
-0.6
-0.8
-1
Sn
Cd
Se
Pb
Sr
Ca
K
Mn
Li
Mg
Pr
U
Nd
Mo
Fe
Th
Ga
Cu
Rb
Zn
Sb
La
Ce
Ru
Ba
As
S
Zr
Al
Ag
Pd
P
Ti
Na

614

615 Fig. S2. Factor Analysis of elemental concentrations (34 elements) in the PO2 core for the
616 two instructive factors. Factors 1 and 4 are anti-correlated with detrital and marine influence,
617 respectively.

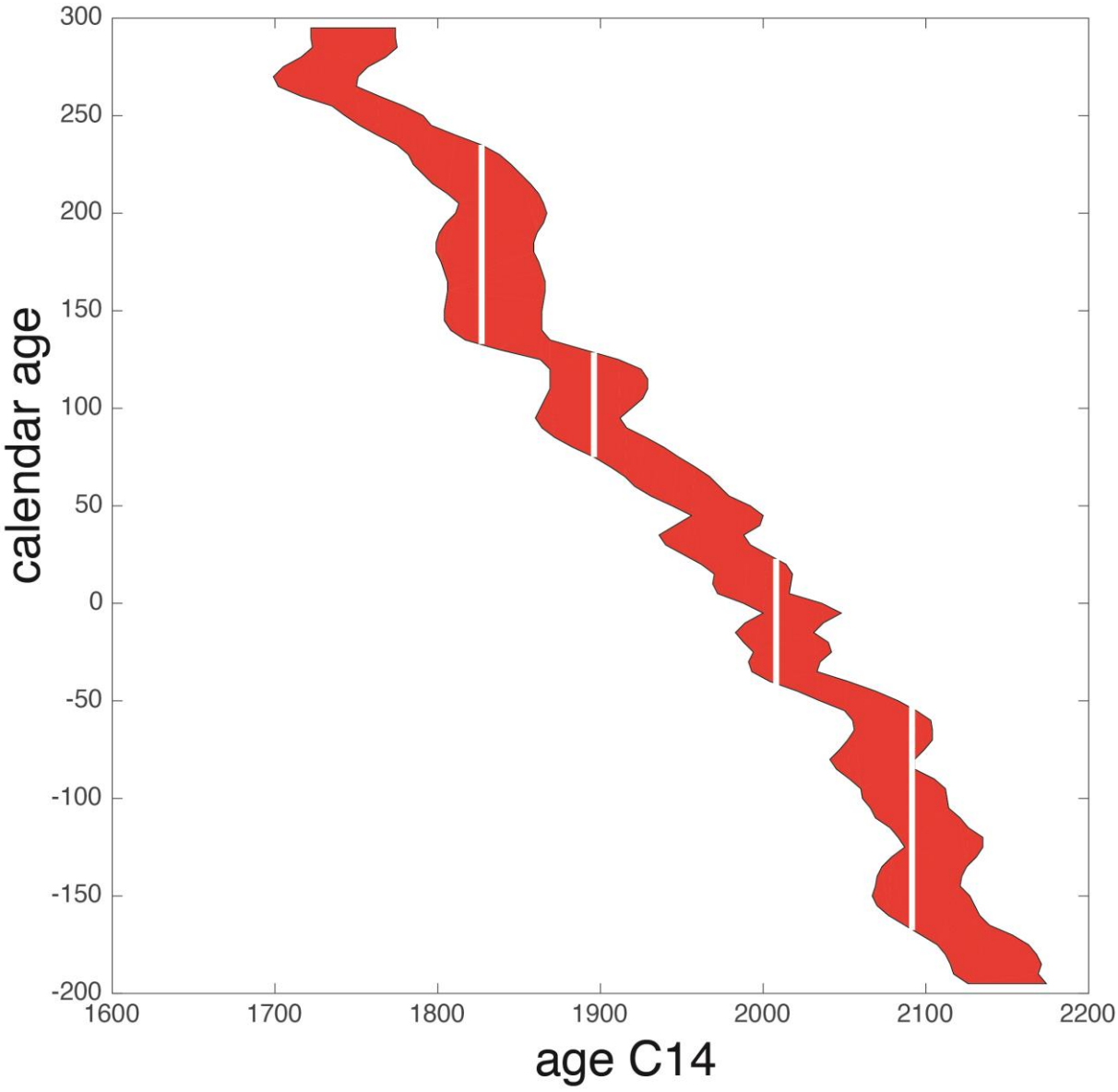

618

619 **Fig. S3.** Illustration of the uncertainties of the ^{14}C dates with ±2-sigma uncertainty (or 95%
620 confidence) intervals. BP ages, calendar years, and uncertainties are from the IntCal13
621 radiocarbon age calibration (31). The white bars emphasize how large the uncertainties can be
622 for some dates. Because the ^{14}C age vs calendar age curve is not single-valued everywhere
623 (one *x* value may correspond to more than one *y* value), the magnitude of the 2-sigma (95%)

confidence intervals on calendar ages varies and occasionally may break into discontinuous segments.

Table S1. ^{14}C dates of cores PO2 and PTXI-3. Ages were calibrated according to the IntCal13 radiocarbon calibration curve (31) using the Clam software (55). The age-depth modeling procedure was done with the Clam software in order to produce model dates with comparable to those from Delile et al. (2). However, the Bayesian age-depth modeling software Bacon (1) provides similar model dates.

1. Blaauw M, Christen JA (2011) Flexible paleoclimate age-depth models using an autoregressive gamma process. *Bayesian Anal* 6(3):457–474.

Table S2. Factor 1 and Factor 4 data of the Factor Analysis done on major and trace element abundances.

Table S3. Pb isotope compositions and T_{mod} (Ma), μ and κ of the two natural components α' and α'' and the anthropogenic component β.

Table. S4. Pb isotope compositions, T_{mod} (Ma), μ and κ, and proportions of the components β, α', α" in the sediment leachates from the PO2 and PTXI-3 cores.

Table. S5. Major and trace element concentrations of the sediments from the PO2 core and Pb concentrations of the sediments from the PTXI-3 core. Values in wt.% for major elements and in ppm for trace elements.